PROCEEDINGS OF SPIE

SPIEDigitalLibrary.org/conference-proceedings-of-spie

Lateral shift mapping metrology for X-ray telescope mirrors

Wisniewski, Hayden, Whalen, Mallory, Heilmann, Ralf, Schattenburg, Mark, Chalifoux, Brandon

Hayden J. Wisniewski, Mallory M. Whalen, Ralf K. Heilmann, Mark L. Schattenburg, Brandon D. Chalifoux, "Lateral shift mapping metrology for X-ray telescope mirrors," Proc. SPIE 11822, Optics for EUV, X-Ray, and Gamma-Ray Astronomy X, 118220X (23 August 2021); doi: 10.1117/12.2594275

SPIE.

Event: SPIE Optical Engineering + Applications, 2021, San Diego, California, United States

Lateral shift mapping metrology for X-ray telescope mirrors

Hayden J. Wisniewski[a], Mallory M. Whalen[b], Ralf K. Heilmann[b], Mark L. Schattenburg[b], Brandon D. Chalifoux*[a]
[a]James C. Wyant College of Optical Sciences, The University of Arizona, 1630 E University Blvd. Tucson, Az USA 85721;
[b]MIT Kavli Instituite for Astrophysics and Space Research, Massachusetts Institute of Technology, 77 Massachusetts Avenue, Cambridge, MA USA 02139

ABSTRACT

Currently, high-resolution X-ray telescope mirrors, such as for the Lynx X-Ray Observatory concept, are measured using a Fizeau interferometer with a cylindrical null corrector. Uncertainties in the null wavefront directly couple into the surface measurement uncertainty, including the axial figure and cone angle variation. We extend the absolute surface metrology method of lateral shift mapping for measuring X-ray telescope mirror segments. Lateral shift mapping involves laterally shifting the surface under test relative to the null to multiple positions. The null wavefront can be extracted from the difference between these shifted measurements, leaving only the surface under test. Accurately extracting quadratic terms of the surface under test requires measuring its tilt during shifting. We will show surface metrology results of optical flats measured by Fizeau-based lateral shift mapping with the required angle measured using an autocollimator and compare these results against a three-flat test. We will show how we plan to extend this method to conical X-ray telescope mirror metrology. The lateral shift mapping method reduces the uncertainty introduced by the cylindrical null, a critical step toward making high-resolution X-ray telescope mirrors.

Keywords: X-ray telescope, Lynx, metrology, absolute metrology, X-ray mirror metrology.

*bchal@arizona.edu

1. INTRODUCTION

Currently the low-spatial frequency height error (figure) of X-ray telescope mirrors is measured using a variety of approaches: X-ray pencil beam[1] or Hartmann[2] metrology, Fizeau interferometry with a refractive or diffractive cylindrical null[3,4,5] (Figure 1), long trace profilometry[6,7], Shack-Hartmann wavefront sensing[8,9], and deflectometry[10]. Fizeau interferometry is particularly useful for quickly making high-precision (sub-nm repeatability) full-surface measurements of segmented X-ray mirrors at atmospheric pressure. However, the cylindrical reference surface or wavefront is difficult to characterize due to its lack of point symmetry. To achieve the Lynx X-ray Observatory concept performance goal of a 0.5 arcsec half-power diameter on axis[11], the mirrors need to be characterized to the 5 nm rms domain[12]. If the reference can only be characterized to this level or worse, it is impossible to tell whether a feature in the interferogram is due to the null or the surface under test (SUT). For systems with point symmetry (flats and spheres), this problem is solved with absolute measurement techniques[13]. These methods provide the surface profile without the uncertainty of manufactured perfectness in the null.

A well-known optical absolute surface metrology method is the three-flat test[13]. Three flats are put through a sequence of measurements and the result is a singular line on each surface that can be known with very low uncertainty. In this method, there is a line along the surfaces that is invariant, and this property is exploited to separate the reference and test surfaces which are added together in the interferogram. The three flat test is a great absolute test for optical flats and has been examined for many years. It has been expanded to measure the entire surface of the flats, not just along the invariant line[14], but it can't be expanded to curved surfaces. Absolute testing has been expanded to spheres through the shift rotation method[15,16]. This method involves obtaining the rotationally asymmetric terms through a surface rotation, and the rotationally symmetric terms through a lateral angular shift. Both methods have their limitations as neither can be expanded to X-ray telescope mirrors, which are acylindrical surfaces that have a small cone angle (~1°) and curved axial profile.

X-ray telescope mirrors are difficult to characterize due to their off-axis parabolic and hyperbolic surface profiles[17]. The acylindrical surface profile implies that the new absolute metrology technique must be viable for curved surfaces without

Optics for EUV, X-Ray, and Gamma-Ray Astronomy X, edited by Stephen L. O'Dell, Jessica A. Gaskin, Giovanni Pareschi, Proc. of SPIE Vol. 11822, 118220X · © 2021 SPIE · CCC code: 0277-786X/21/$21 · doi: 10.1117/12.2594275

point symmetry. Here we present lateral shift mapping, an interferometric absolute surface measurement for X-ray telescope mirrors. This method was studied in 2010 for flat surfaces[18], and the work here is a confirmation of the method that was proposed then. We recreate this method for flat surfaces and present requirements and plans to expand this method to X-ray telescope mirrors. A rendering of an X-ray mirror can be seen in Figure 1. X-rays entering the telescope will travel along the z-direction and reflect off the mirror, meaning the curve along the z-direction (axial profile) and its relation to the optical axis (cone angle) are crucial for system performance[11]. An X-ray telescope mirror metrology system should therefore measure axial profile and cone angle variation, with special attention to the quadratic term in the axial profile (Figure 1). The lateral shift mapping method presented here aims to measure the quadratic and higher-order terms with the goal of extending this to X-ray mirrors with similar accuracy.

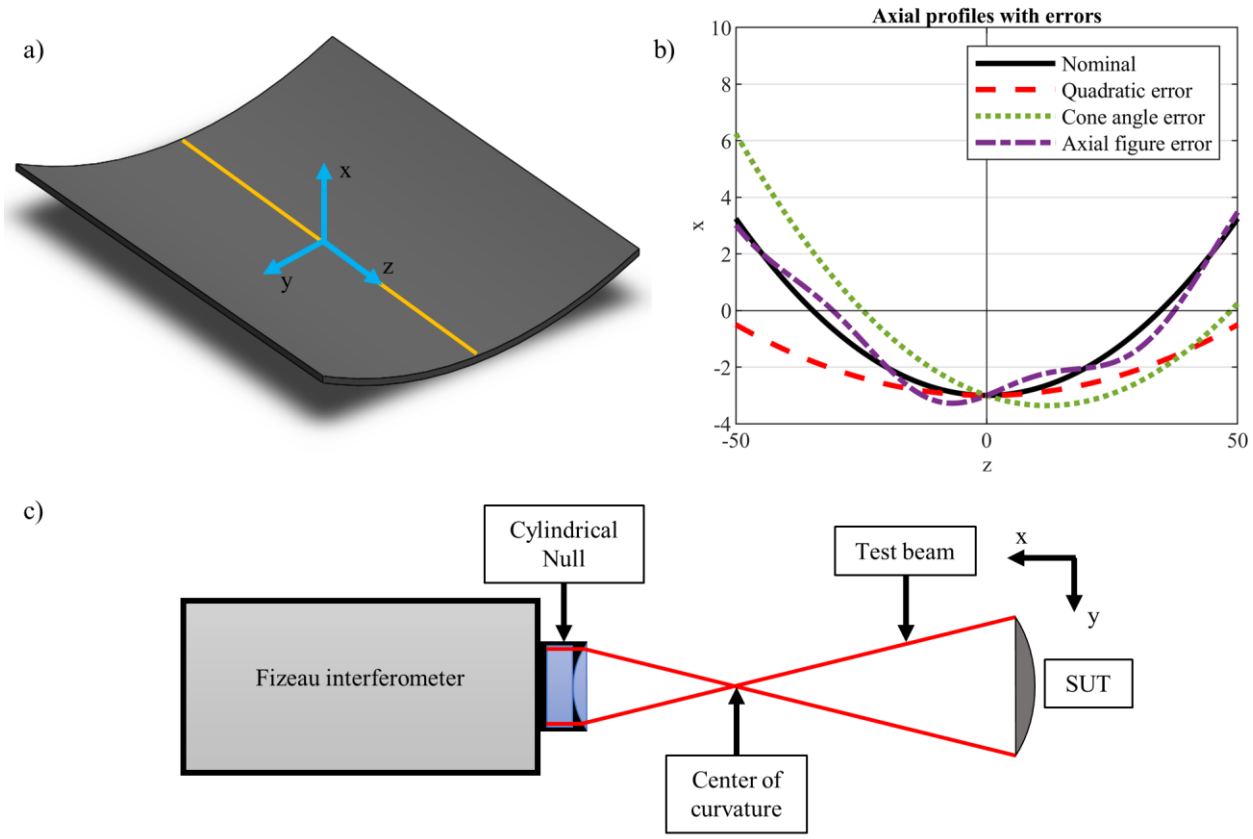

Figure 1. a) Rendering of an X-ray telescope mirror segment with coordinate frame. **b)** An illustration showing various types of errors that affect X-ray telescope performance. **c)** A Fizeau interferometer with cylindrical null. Due to the single line of symmetry and difficulty of manufacturing, cylindrical nulls are extremely difficult to characterize. Lateral shift mapping aims at easing the characterization of this cylindrical null to allow for quicker more accurate measurements of X-ray telescope mirrors.

2. METHOD

In lateral shift mapping, one of the optical surfaces is held static (relative to the interferometer) and the other surface is shifted perpendicular to the optical axis of the interferometer[18]. Absolute surface information can only be extracted along the direction of shifting, but the surface of both the static and shifted surfaces can be extracted. In this experiment the reference and test surfaces are transmission flats, in a cylindrical system for X-ray mirrors, the reference will be a cylindrical null wavefront and the SUT will be an X-ray mirror.

2.1 Matrix surface extraction

A measurement by the Fizeau will be a surface profile that contains both the imperfections of the SUT and the reference surface. The measurement can be described as

$$h_{i,j} = S_i + R_i \tag{1}$$

where h is the surface height at position index i, j is the shift index (0 for the first measurement), S is the actual height of the SUT, and R is the actual height of the reference. The SUT then needs to be shifted by an integer number multiplied by the projected pixel size of the interferometer CCD[19]. This then gives a height measurement of

$$h_{i,j+1} = S_{i+1} + R_i \tag{2}$$

where the surface index i is in reference to the interferometer pixel index. In each measurement, contributions due to the reference surface will stay the same in every measurement and contribution by the SUT will move by the integer number of pixels every shift (Figure 2). This relationship is true for every pixel along that line. This creates a linear system of equations that can be described in matrix form as

$$K \bullet \vec{z} = \vec{m} \tag{3}$$

where z is a vector of the actual surface heights of the reference and SUT at each surface index and m is the collection of all measurements at each pixel. Expanding equation (3) gives

$$\begin{bmatrix} 1 & 0 & \cdots & 0 & 0 & 1 & 0 & \cdots & 0 & 0 \\ 0 & 1 & \cdots & 0 & 0 & 0 & 1 & \cdots & 0 & 0 \\ & & \ddots & & & & & \ddots & & \\ 0 & 0 & \cdots & 0 & 1 & 0 & 0 & \cdots & 0 & 1 \\ 1 & 0 & \cdots & 0 & 0 & 0 & 1 & \cdots & 0 & 0 \\ 0 & 1 & \cdots & 0 & 0 & 0 & 0 & 1 & \cdots & 0 \\ & & \ddots & & & & & & \ddots & \\ 0 & 0 & \cdots & 1 & 0 & 0 & 0 & \cdots & 0 & 1 \\ 0 & 0 & \cdots & 0 & 1 & 0 & 0 & \cdots & 0 & 0 \\ 1 & 0 & \cdots & 0 & 0 & 0 & 0 & 1 & \cdots & 1 \\ & & & & & \vdots & & & & \end{bmatrix} \begin{bmatrix} z_{R,1} \\ z_{R,2} \\ \vdots \\ z_{R,N-1} \\ z_{R,N} \\ z_{S,1} \\ z_{S,2} \\ \vdots \\ z_{S,N-1} \\ z_{S,N} \end{bmatrix} = \begin{bmatrix} m_{1,1} \\ m_{1,2} \\ \vdots \\ m_{1,N} \\ m_{2,1} \\ m_{2,2} \\ \vdots \\ m_{2,N} \\ \vdots \\ m_{M,1} \\ m_{M,2} \\ \vdots \\ m_{M,N} \end{bmatrix}, \tag{4}$$

where in the z-vector, R and S represent the reference and SUT respectively from pixel 1 to pixel N, and in the m-vector, each entry, $m_{p,q}$, is the value of the p^{th} measurement at the q^{th} pixel, from measurement 1 to M and pixel 1 to N. The **K** matrix is then built to relate the z vector to the m vector using the principles behind equations (1) and equation (2). The z vector is of length $2N$ and the m vector is of length MN, meaning the **K** matrix is of size $MN \times 2N$. Between the 4^{th} and 5^{th} numeric column in equation (4) is the transition of multiplying by the reference pixels in the z-vector to multiplying by the SUT pixels in z-vector. Both halves are identity matrices, except the SUT half of the K matrix must shift right and up one after every N rows to reflect the physical shift of the system. This can be seen between the 3^{rd} and 4^{th} numeric row and 7^{th} and 8^{th} numeric row of equation (4), which are transitions from measurement 1 to measurement 2 and from measurement 2 to measurement 3. A diagram showing how values in the z vector relate to values in the m vector can be seen in Figure 2.

Since **K** is not square it cannot be inverted. Instead, equation (3) can be solved using a well-known least mean squared error method of the Moore-Penrose inverse. Equation (3) is thereby solved

$$\vec{z} = (K^T K)^{-1} K^T \vec{m} = K^+ \vec{m}\,, \tag{5}$$

from which we can extract the surface profile of both the reference and SUT. When two measurements (i.e., only one shift) are made, **K** is invertible. As more measurements are made it becomes an over-defined set of equations, but it has more values that contribute to the least mean squared approach. This allows errors due to vibrations and air currents to be averaged out.

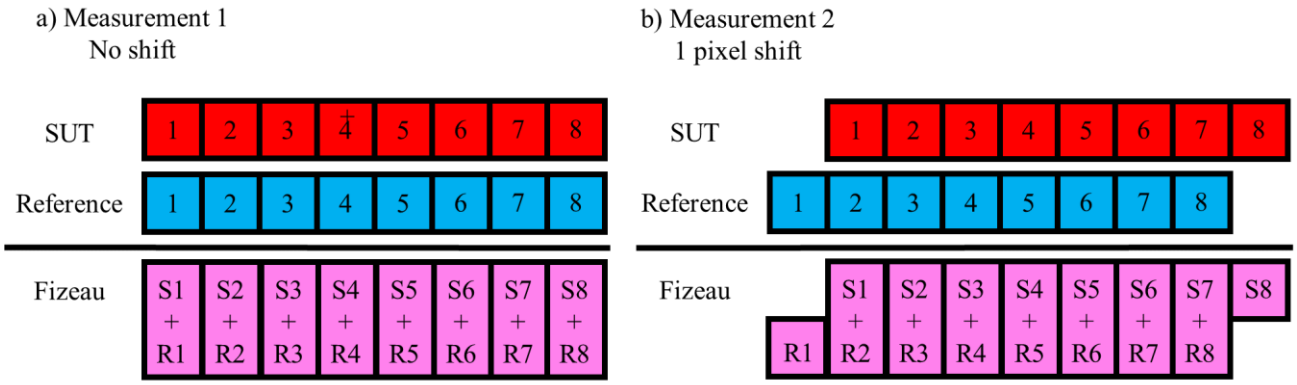

Figure 2**.** Each surface measurement is a pixel-by-pixel addition of the SUT and the reference. Once shifted, the surfaces are now added together at different indices. This allows the system of shifts to be described by equations (1) - (3) and ultimately solved. Locations where only one surface has a value will not have a value in the Fizeau surface profile, thus information is lost at the edges if the SUT is larger than the reference. This method can also be performed with multipixel shifting[19] and the **K** matrix must be built to reflect this.

2.2 Removing quadratic errors

The matrix extraction method can be thought of as an integration of slope across the surface, therefore linear tilt errors in the measurements will become quadratic errors in the final extracted surface profile. In lateral shift mapping, stage rotations inevitably occur during lateral shifting. These tilts produce interferogram tilt fringes that can be removed, but quadratic profiles of the SUT or reference would *also* produce tilt fringes during shifting, and the two cannot be distinguished without an external independent measurement of the stage tilts (or a reference or SUT with perfectly-characterized quadratic error). This can be dealt with in two ways. The first is to fit a quadratic model to the data and subtract it out, artificially ignoring this term. The second method uses an autocollimator to measure the relative tilt introduced between two measurements as the SUT shifts. An autocollimator is placed with its optical axis perpendicular to the optical axis of the interferometer. As the SUT shifts towards it, the autocollimator will measure the angle that the interferometer would see as a tilt. Using this measurement of angle, the relative tilts between two measurements can be removed, which would eliminate the quadratic error in the system. This method relies on an autocollimator that has a low noise floor and low drift. This blindness to the quadratic without an external measurement system is a problem specific to lateral shift mapping. Long-trace profilometry is a metrology method that is not blind to this term[7]. Standard interferometry with an uncharacterized reference or null is of course blind to quadratic as well as higher-order terms.

3. EXPERIMENTAL SETUP

A Zygo Verifire Fizeau interferometer was used to obtain the surface profiles of the flats. Two Zygo optical transmission flats rated at λ/20 P-V (λ = 633 nm) were used as the reference and test surface. An optical flat was connected to the head of the interferometer, becoming the reference surface. The other optical flat was inserted into a Zygo 5-axis mount. This mount was on an Aerotech XY130 stage that was able to shift perpendicular to the optical axis (x-axis in Figure 3). To shift according to the method prescribed, the optical axis translation was not needed, rather the SUT was shifted in the x-direction.

To measure the relative tilts between measurements, an Elcomat 3000 autocollimator was placed along the x-axis. The relative tilts would be tilts of the SUT about the y-axis. This also required a mirror to be rigidly attached to the SUT and

perpendicular to the optical axis for the autocollimator. A mount was designed that attached to the face of the Zygo 5-axis mount that holds the SUT in bayonet mounts. This ensured there was minimal hardware between SUT and autocollimator mirror.

We found that vibrations and air currents were limiting sources of noise. To mitigate air currents, an air box was constructed around the system. To reduce vibrational noise, the system was moved to a quiet environment and onto a vibration isolation table. The Fizeau interferometer, autocollimator, and translation stage were all controlled remotely, which allowed it to operate without a user creating vibrations in the lab. To lessen vibrations due to the system shifting, the stage would shift and a time interval would elapse to allow the system to settle before the measurements of the interferometer and the autocollimator would begin. The system diagram can be seen in Figure 3 and the physical set up can be seen in Figure 4.

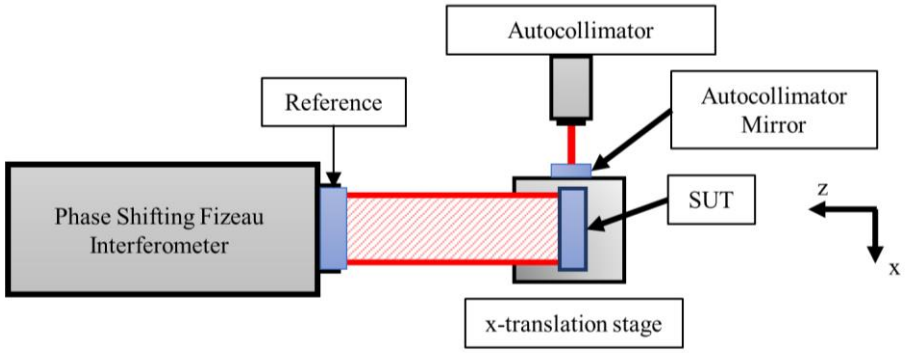

Figure 3. Plan view of experimental setup. The SUT was shifted on the translation stage in the x direction while the autocollimator measured rotations of the SUT about the y axis, which create quadratic error in the extracted surface. Tilts about the z axis are minute and will have no effect on the system. The interferometer, autocollimator, and translation stage were controlled remotely to avoid the operator adding vibrations to the measurement.

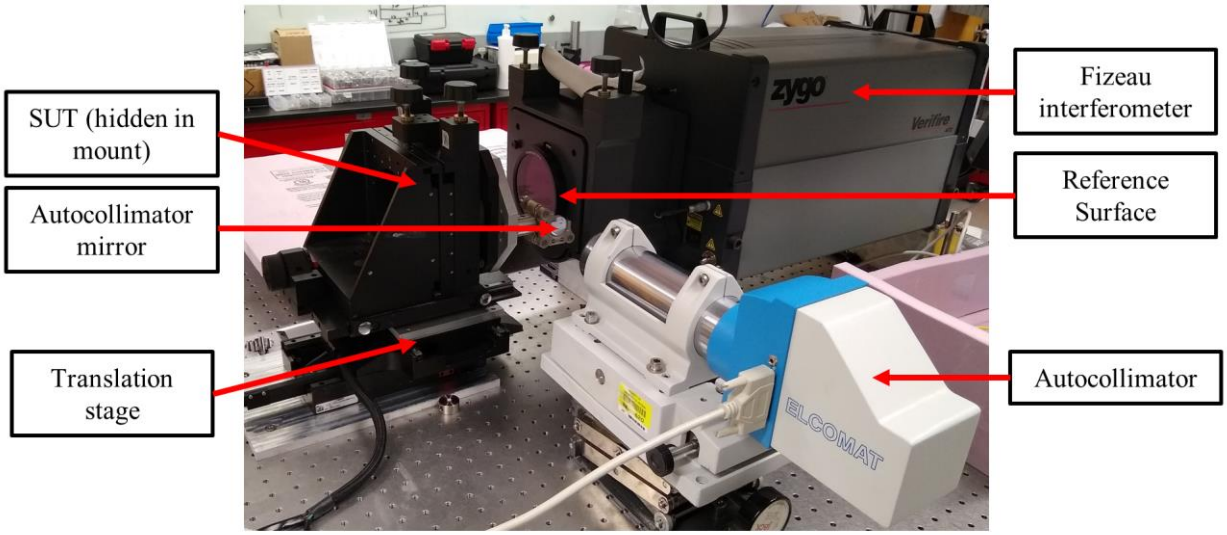

Figure 4. Experimental set up with the autocollimator in place. The SUT on the translation stage moves perpendicular to the optical axis. The SUT is hidden from view in its mount. An airbox was constructed around this set up before data taking to minimize airflow in the optical cavity.

4. RESULTS

Here we show the results of extracting this data two ways, depending on how a quadratic error is removed. This quadratic error is due to angular rotations about the y-axis (Figure 3) as the surface is shifted along the x-axis. The results shown are using the same set of data taken with the Fizeau interferometer. The final surfaces are the result of averaging 25 sets of measurements, and each set was comprised of 40 shifts with a shifting distance of 2 pixels each (100 μm per pixel). To minimize noise from vibrations and air currents, the interferogram was averaged 100 times per measurement and the autocollimator collected 1000 data points per measurement. With these high number of averages per measurement, the full 25 sets of measurements took 36 hours in total, but that time scale will be reduced in the future by optimizing the averaging and measuring in a low noise environment. A three-flat test was also performed on the same day using a third optical flat. This was to ensure that the comparison three-flat test data was taken under the same environmental conditions. Three separate three flat tests were performed and averaged together to avoid any environmental effects, such as vibrations. A low pass spatial frequency filter was applied to filter all signals with a spatial wavelength smaller than 1 mm to eliminate effects due to scattering. The filter was applied to both lateral shift mapping measurements and three-flat test data.

4.1 Artificial removal of quadratic error

The artificial quadratic term extraction involves fitting a quadratic model to the data and then subtracting this model from the data. This artificial quadratic extraction was done to both the lateral shift mapping surface and the three-flat test surface to ensure that any post processing done was done equally to both surfaces. Therefore, the power term is missing in the three flat test profile as well. This is to test whether the lateral shift mapping method is accurate for higher-order terms.

A comparison between the three-flat test measurement and the lateral shift mapping method can be seen in Figure 5. The rms difference between the two measurements is 0.53 nm for the SUT and 0.68 nm for the reference. This great agreement between the two surfaces demonstrates that lateral shift mapping is a valid absolute measurement technique when the quadratic term is left out. This also means that with the power term left in the extraction, it is possible to extract the surface of the two flats as long as the method for dealing with the quadratic error is precise enough.

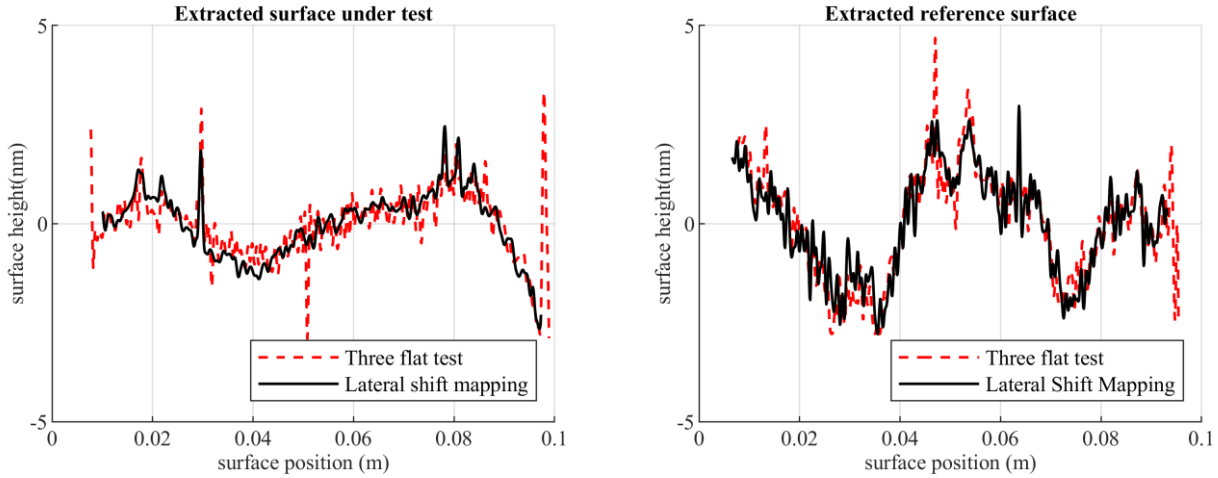

Figure 5. SUT (*left*) and reference surface (*right*) when extracted by the three-flat test and by lateral shift mapping with the quadratic term artificially removed. The rms difference between the three-flat test method and lateral shift mapping method for the SUT was 0.53 nm and for the reference surface was 0.68 nm. These extractions are without autocollimator data, meaning that all quadratic error was removed by fitting a quadratic model to the final surface and subtracting it out. This removes all knowledge of the power along the line extracted.

4.2 Autocollimator removal of quadratic error

Using autocollimator measurements, we remove the relative tilts of the reference surface and SUT before processing the data. For each surface measurement, the autocollimator gathered and averaged 1000 points of data to minimize random error. In a set, which has 40 shifts/measurements, the autocollimator measurement was used to remove any relative tilt

by subtracting a best fit line of angle times surface length. If there was no error in the autocollimator, all surfaces would then have the same linear trend as the first line, with different surface values because of the shifts.

The extracted surfaces are shown in Figure 6 and a clear quadratic trend can be seen. Since this data is the same as the artificial power extraction, the surface information is present, just hidden by the quadratic term. This quadratic term is due to either angle measurement errors or unmeasured relative tilts between the reference and SUT. The surfaces have an rms difference of 18.90 nm for the reference surface and 20.07 nm for the SUT when compared to the Three flat test. The source of the noise must be found and reduced for this method to prove viable for X-ray telescope mirrors.

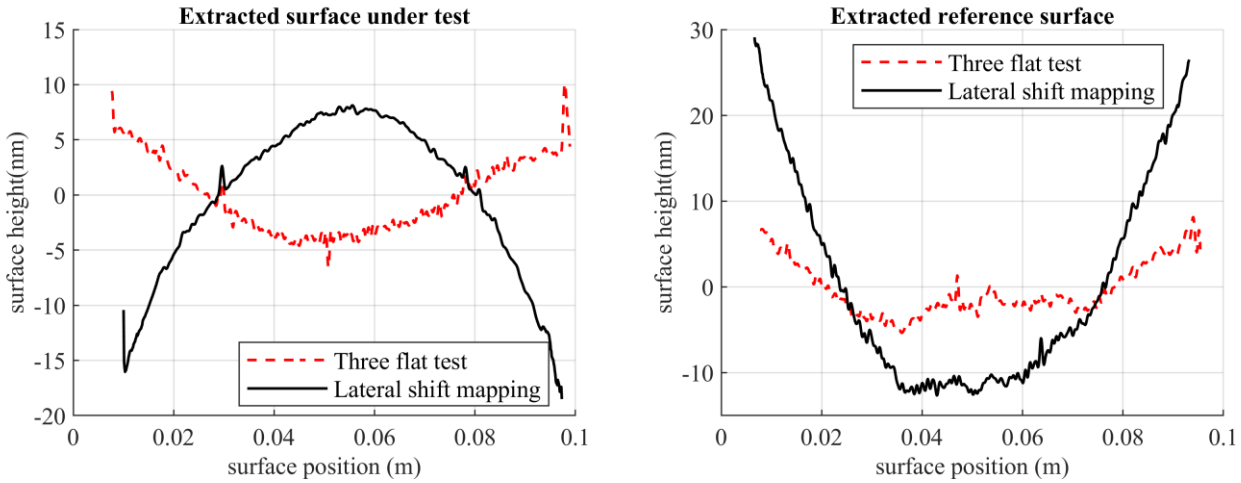

Figure 6. SUT (*left*) and reference surface (*right*) when extracted by the three-flat test and by lateral shift mapping when the tilt in the mirror is measured and removed with an autocollimator. The rms difference between the three-flat test method and lateral shift mapping method for the SUT was 20.07 nm and for the reference surface was 18.90 nm, which is a large error compared to removing the quadratic artificially (Figure 5). This is due to a drift in the autocollimator which will be discussed in section 4.3 Sources of error.

4.3 Sources of error

The largest source of measurement error, by far, is in the relative tilt measurement between the reference and SUT, as evidenced by the quadratic error in the autocollimator removal method. The autocollimator random noise was 260 nrad rms over about 78 seconds. We simulated measurements with this error included, and the resulting quadratic error was about 1 nm, suggesting this is not a cause of the observed quadratic error. The error is likely a product of drift somewhere in the system. Unmeasured tilt error could have been introduced by the reference surface (not monitored during this experiment) drifting in the tip tilt mount of the interferometer, or the autocollimator mirror mounted to the SUT drifting in reference to the SUT. It was discovered that in the direction that we were measuring (rotations about the y-axis) the autocollimator measured a linear drift of ~150 nrad/hr (Figure 7). Simulating measurements with 150 nrad/hr tilt produced quadratic errors of about 90 nm rms. This is much larger than the error that we measure. An autocollimator drift of 35 nrad/hr produces an error of 20 nm rms, which suggests angular drift on this scale as a plausible cause of the quadratic error. It is possible that there is an unobserved drift on the order of 35 nrad/hr (for example, the unmonitored reference surface could be drifting in its mount) which is masked by the larger 150 nrad/hr drift we did measure and accounted for in our analysis. In future experiments the source(s) of this drift, observed and possibly unobserved, will need to be determined and mitigated to allow the autocollimator power extraction method to work at an acceptable level. Faster measurement, or different measurement ordering strategies may help mitigate effects of drift.

The effect of temperature on the system has not yet been explored, but at these height scales (~5 nm rms) it can be assumed that thermal expansion and contraction of the system will have a detrimental effect on the system. In the future the air box will be replaced with a thermally controlled container.

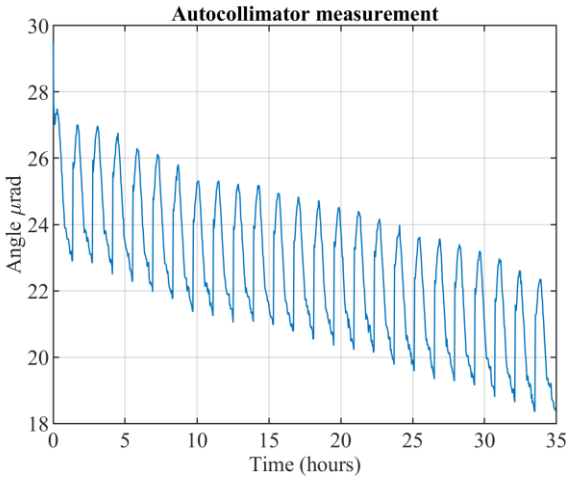

Figure 7. Angle measured by the autocollimator over the course of the measurement. The trend has a slope of -150 nrad/hr. Each sinusoidal period is the system shifting from the starting to ending position and then resetting.

5. FUTURE WORK

The first item that needs to be addressed with this project is the drift in the autocollimator measurement. This will allow us to confirm that we can absolutely extract the SUT while knowing the power term. Once that is confirmed we can continue on to expanding this method to curved X-ray telescope mirrors.

Expanding to curved X-ray mirrors will require the design of systems around the interferometer. The first system will be a cylindrical null. This null will most likely be composed of 2 cylindrical lenses and fill the full 4-inch aperture. This system of cylindrical lenses will be used to generate a cylindrical reference wavefront similar to the one seen in Figure 1.

A z-theta stage is being designed to move the SUT in discrete pixel steps in the orthogonal z and theta directions independently (Figure 8). Motion in the z-direction will be provided by a linear stage, placed on an air bearing platform so that it can be moved by the theta control scheme. Motion in the theta direction will involve a theta stage at the center of curvature, which is then connected to the floating z-stage via a radial arm. Analysis for the z-direction will be very similar to the analysis presented here. An autocollimator must still be present to measure the tilt as the z-stage moves up and down because the quadratic term along those surface profile lines will determine the mirror's effectiveness. Figure 8 shows a concept as to how the autocollimator can be implemented in the scanning system by passing the beam through the center of the theta stage. This configuration will allow for a full surface profile to be measured with a known power term along the z-direction.

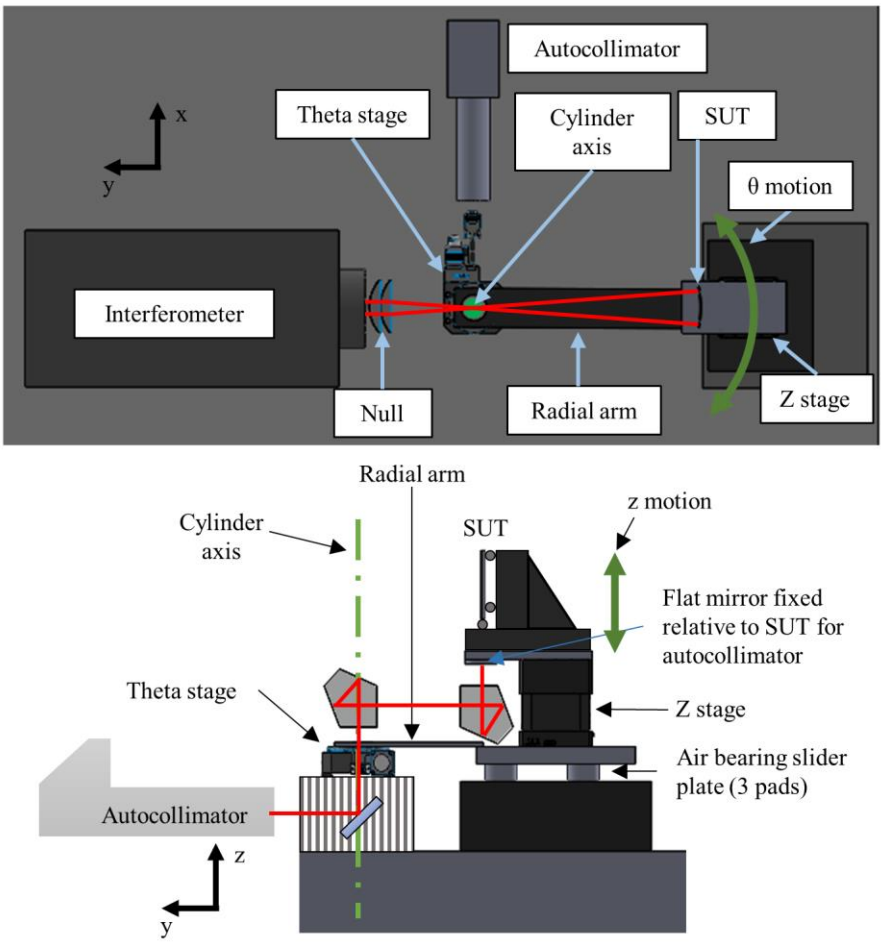

Figure 8**.** Design of z-theta stage for absolute measurement of X-ray telescope mirrors. Top view *(top)* shows test beam passing through the null, converging at the center of curvature and reflecting off of the SUT. This will allow the SUT to shift a discrete number of pixels in the theta direction without affecting any other rigid body motions. Side view *(bottom)*, excluding the interferometer, shows how the theta portion will slide on an air bearing plate, moved by the theta stage through the radial arm. It also shows how the autocollimator measures the angle of the SUT as it translates in the z-direction. The autocollimator's optical axis will be along the x-axis (as in the top view), but shown along the y-axis here to demonstrate how its beam will be folded to the mirror under the SUT. Pentaprisms are not shown in the top view.

6. CONCLUSION

We presented results demonstrating the ability to absolutely measure a surface profile of an optical flat using lateral shift mapping if the power term is artificially removed. We confirmed this by comparing results for lateral shift mapping against the results for a three-flat test, a well-known absolute metrology technique. The rms difference between the surface profiles of the two methods were 0.53 nm for the SUT and 0.68 nm for the reference surface. This result confirms that the surface profile, without the power term, can be extracted using this method. We also showed results for extracting the surface, but eliminating the power term by removing relative tilts with autocollimator measurements. When compared against a three flat test the surfaces have an rms difference of 20.07 nm for the SUT and 18.90 nm for the reference surface. It was found that the large difference in the two methods is due to long term drifting of the autocollimator. This error source will be addressed before continuing on to curved optics.

We finished by presenting a concept for a z-theta stage that will allow lateral shift mapping to be extended to curved optics, specifically acylindrical optics. This will allow cylindrical nulls, which are historically difficult to measure, to be characterized to the 5 nm rms domain. Well characterized cylindrical nulls will aid in the characterization of X-ray

telescope mirrors, with the overall impact of aiding the effort to create a diffraction limited X-ray telescope like the Lynx X-ray Observatory concept.

7. ACKNOWLEDGEMENTS

We would like to thank Will Zhang at NASA Goddard Space Flight Center and David Windt at RXO for engaging conversations while developing this method. We want to thank Heng Zuo at MIT for giving us access to the translation stage used. This work was funded by NASA grant 80NSSC20K0907.

REFERENCES

[1] G. Vacanti, N. M. Barrière, M. J. Collon, E. Hauser, L. Babić, A. Bayerle, D. Girou, R. Günther, L. Keek, B. Landgraf, B. Okma, S. Verhoeckx, M. Vervest, L. Voruz, M. Bavdaz, E. Wille, M. Krumrey, P. Müller, and E. Handick, "X-ray testing of silicon pore optics," in Proc. SPIE 11119, p. 111190I. (2019).

[2] T. T. Saha, K.-W. Chan, J. R. Mazzarella, R. S. McClelland, P. M. Solly, W. W. Zhang, V. Burwitz, G. Hartner, M.-M. L. Caria, and C. Pelliciari, "Analysis of the NGXO telescope x-ray Hartmann data," in Proc. SPIE 10699, p. 1069952 (2018).

[3] J. P. Lehan, T. Hadjimichael, and C. Skocik, "Testing of the mirrors for the Constellation-X spectroscopy x-ray telescope with a refractive null," in Proc. SPIE, Vol. 6688, pp. 668819-668819–8 (2007).

[4] J. P. Lehan, M. Atanossova, K.-W. Chan, T. Hadjimichael, T. T. Saha, M. Hong, W. W. Zhang, and P. Blake, "Progress toward a complete metrology set for the International X-ray Observatory (IXO) soft x-ray mirrors," in Proc. SPIE, Vol. 7437, pp. 74370R(2009).

[5] Y. Soong, T. Okajima, P. J. Serlemitsos, S. L. Odell, B. D. Ramsey, M. V. Gubarev, M. Ishida, Y. Maeda, R. Iizuka, T. Hayashi, Y. Tawara, A. Furuzawa, H. Mori, T. Miyazawa, H. Kunieda, H. Awaki, S. Sugita, K. Tamura, K. Ishibashi, T. Izumiya, S. Minami, T. Sato, K. Tomikawa, N. Kikuchi, and T. Iwase, "ASTRO-H Soft X-ray Telescope (SXT)," in Proc. SPIE, Vol. 9144, p. 914428 (2014).

[6] H. Li, P. Z. Takacs, and T. Oversluizen, "Vertical scanning long trace profiler: a tool for metrology of x-ray mirrors," in Materials, Manufacturing, and Measurement for Synchrotron Radiation Mirrors (International Society for Optics and Photonics, Vol. 3152, pp. 180–188 (1997).

[7] M. V. Gubarev, T. Kester, and P. Z. Takacs, "Calibration of a vertical-scan long trace profiler at MSFC," in Proc. SPIE, Vol. 4451, pp. 333–340 (2001).

[8] R. Allured et al., “Measuring the performance of adjustable x-ray optics with wavefront sensing,” Proc. SPIE 9144, 91441D (2014).

[9] C. R. Forest, C. R. Canizares, D. R. Neal, M. McGuirk, and M. L. Schattenburg, "Metrology of thin transparent optics using Shack-Hartmann wavefront sensing," Opt. Eng 43(3), 742–753 (2004).

[10] K. Kilaru, B. D. Ramsey, W. H. Baumgartner, S. D. Bongiorno, D. M. Broadway, P. R. Champey, J. M. Davis, S. L. O’Dell, R. F. Elsner, J. A. Gaskin, S. Johnson, J. K. Kolodziejczak, O. J. Roberts, D. A. Swartz, and M. C. Weisskopf, "Full-shell x-ray optics development at NASA Marshall Space Flight Center," J. Astron. Telesc. Instrum. Syst. 5(2), (2019).

[11] Gaskin, J. A. et al., “Lynx X-Ray Observatory: an overview,” J. of Astronomical Telescopes, Instruments, and Systems. 5(2), (2019).

[12] W. W. Zhang, K. D. Allgood, M. Biskach, K.-W. Chan, M. Hlinka, J. D. Kearney, J. R. Mazzarella, R. S. McClelland, A. Numata, R. E. Riveros, T. T. Saha, and P. M. Solly, "High-resolution, lightweight, and low-cost x-ray optics for the Lynx observatory," J. Astron. Telesc. Instrum. Syst. 5(2), 021012 (2019).

[13] G. Schulz and J. Schwider, “IV Interferometric Testing of Smooth Surfaces,” Progress in Optics 13, 118-140 (1976)

[14] U. Griesmann, “Three-flat test solutions based on simple mirror symmetry,” Appl. Opt. 45(23), 5856-5865 (2006)

[15] D. Su, E. Miao, Y. Sui, and H. Yang, "Absolute surface figure testing by shift-rotation method using Zernike polynomials," Opt. Lett. 37, 3198-3200 (2012)

[16] W. Song, F. Wu, X. Hou et al. “Absolute calibration of a spherical reference surface for a Fizeau interferometer with the shift-rotation method of iterative algorithm,” Opt. Eng. 52(3), (2013).

[17] L. P. VanSpeybroeck, and R. C. Chase, "Design Parameters of Paraboloid-Hyperboloid Telescopes for X-ray Astronomy," Appl. Opt. 11, 440-445 (1972).

[18] E. E. Bloemhof, “Absolute surface metrology by differencing spatially shifted maps from a phase-shifting interferometer,” Opt. Lett. 35(14), 2346-2348 (2010).

[19] E. E. Bloemhof, “Absolute surface metrology with a phase-shifting interferometer for incommensurate transverse spatial shifts,” Opt. Lett. 53(5), 792-797 (2014).